Coreless fiber refractive index sensor in terms of intensity sensing and wavelength shift

Dhiya A. Fenjan, dhiyaf401@uowasit.edu.iq,
Bushra R. Mahdi Boshera65m@gmail.com
Hashim A. Yusr hashim@uowasit.edu.iq

ABSTRACT

A multimode no core fiber (NCF) -based refractive index interferometric (RI) sensor has been demonstrated through experiment. Coreless fibers are directly exposed to environmental factors. The output spectrum changes with the refractive index, type, and contraction of the ambient medium such as Magnesium permanganate. The Mach-Zehnder optical fiber sensor had a 523 nm/RIU sensitivity, and when graphene oxide was coated on top of the gold layer, the sensitivity rose to 950 nm/RIU. Either optical density contrast or wavelength shifting was used to achieve this increase in sensitivity. Coreless fiber is a weakly oriented multi-mode fiber with an index profile when the environment around the sensor is lower than that of a non-core fiber that has single-mode fibers that are spliced at both ends of the coreless fiber segment. As a result, it takes on the shape of the classic (SM-MM-SM) fiber structure but is bigger.

Keywords:

Introduction

Sensors that detect changes in the refractive index (RI) and concentrations of liquids or gases have been worked in this field by many researchers in various uses such as industry and environmental sciences. It was characterized by its small size, light weight, low cost, fast response time, high sensitivity, unaffected by electromagnetic fields, and its ability to work in hazardous and chemical environments [1,2], fiber-optic methods in particular have been actively researched for a long time. There have been several fiber-optic RI sensing designs proposed up to this point. Among these are normal (SMFs) with smaller cladding diameters [3], waisted multimode fiber (MMF) tips [4, 5], High Numerical Aperture (NA) curved multimode plastic fiber, double channel single mode optical fiber bend [6], fiber Bragg (FBGs) [7], side polish fibers [8,] waist-deformed fiber tapers manufactured by [9], and heterostructures created by splicing through the use of surface plasmon resonance, thin film metallic layers coated on the sensor's surface have been used to greatly enhance sensitivity and resolution [14].A variety of microstructures, including Fabry-Perot interferometers and Mach-Zehnder interferometers, have also been constructed [15]. In this study, sensing methods based on optical intensity contrast or wavelength shift have been used to support the general execution of the RI shift sensor due to the Mach-Zehnder No core optical fiber.

Principle of Operation

Based on the distribution of refractive indices, step type and gradual type fibers can be discriminated. In this study, the single-mode(SM)- no-core -single-mode (S-NC-S) step refractive index wide detection sensor was discussed . The abrupt transition the glass cladding is surrounded by a fiber core is referred to as a "step type refractive index multimode fiber" in this phrase. An SNS sensor with GO sensitization is designed as shown in Figure(1) . Based on the distribution of refractive indices, Step type and gradual type of

fibers are two categories of it.. This essay discusses the action An area of NCF is fused on both sides with a piece of SMF, then covered with GO film, with the surrounding solution of the measured ingredient serving as cladding. The NCF can be viewed as a weakly guided multi-mode fiber (MMF) with step RI distribution if the measured substance's RI is lower than the NCF's and the difference is not statistically significant. This structure is identical to the structure of the conventional SMS fiber.

Several higher-order modes will be activated and periodic light focus, or the self-image phenomenon, will be produced in the NCF when incident light is linked from single mode fiber. When the fiber structural parameters stay constant, the energy distribution along the direction of propagation of the fiber is distinct. When the incident light wave is continuous, wavelength and energy are directly correlated with one another, resulting in a certain transmission spectrum. Due to interference between different modes, the transmission spectrum will exhibit a peak or trough in interference depending on the amount of energy present at a specific wavelength.

The suggested sensing head, which is a No core (MMF) section that has been probed and spliced between two SMFs, is illustreted in figure (1). The No core is a multie mode fiber(MMF) consists of a rod of pure silica with n_{ncf} is 1.444, an optical spectrometer (Ocien 2000), and a 650 nm laser source.The theory underpinning the SMS-based fiber structure idea indicates that various multi modes are excited as the a bright field propagates throughout the input SMF. The light beam will therefore propagate along the remaining MMF segment, accumulating the differential phases between the modes.

Figure (1) Schematic diagram expermintal work of coreless fiber sensor.

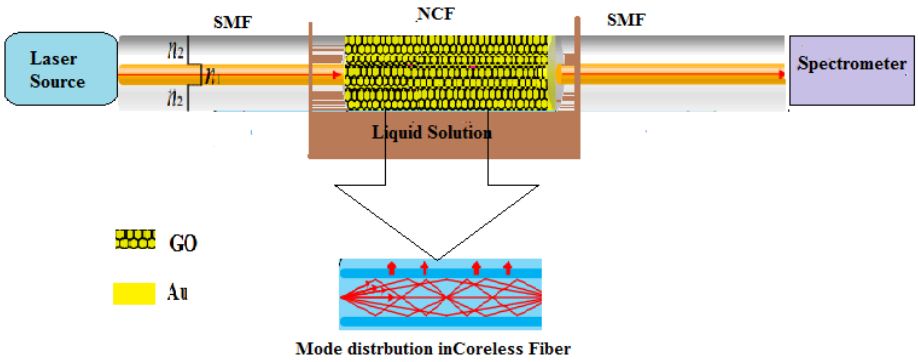

The field profile worldwide keeps its symmetry over the propagation direction even if it moves along the MMF section [16]. Consequently, near the termination of an L-length MMF, various field profiles correspond to various propagation lengths. A number of periodic planes, among which are plans with self-portraits in them (SI) occurs, are also where field condensation occurs [17,18]. In order to get the self-imaging distance (Zi), which is the distance at which the illumination at the MMF section's input is identical at its output in amplitude and phase for a certain wavelength, use the formula

$Z_{i=} 4 (D^2) * (n_{core}) / \lambda$

Where(D) and (n_{core}) are, respectively, the core RI and MMF diameter, and is the operating wavelength, the field profile worldwide fluctuates over the MMF section but stays dispersed symmetrically along the route of transmission. Contrary to the fractional (not self-imaging) planes, where one may assume constructive interference between the two successive modes that were excited with the highest coupling efficiency, in this case the light field condensation in a specific plane is caused by constructive interference between the various guided modes. It should be stressed that only the original self-image (and its multiples) will have the fewest losses and be used in this study.

Our sensor head's operational mechanism is powered by RI fluctuations by the wavelength peak produced by the No core

(MMF) used, which, in theory, will be sensitive to the cladding (in this case, the liquid plays a role in this).

Our sensing head's No core(MMF) experiences a (SI) phenomenon that lasts for a predetermined amount of time and generates a clearly clear wavelength peak that , Sensitive in theory to changes in the cladding's RI (in this case, the liquid's role).

Result and Discussion

Figure (2) displays the intensity spectrum shift for various magnesium permanganate solution concentrations. Concentration-dependent changes in the refractive index, intensity, and shift towards the peak of longer wavelengths all occur as concentration rises.

.

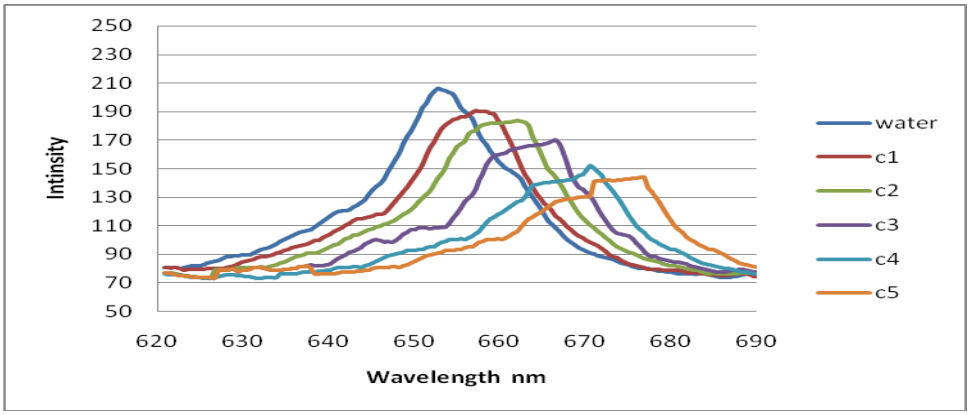

Figure (2) Relationship of intensity of the transmitted light with the wavelengths through the sensor in the Magnesum Brmngnate solution .

The transmission valley in Figure 3 advances in the direction of long wavelengths while the depth gradually deepens as a result of the growing RI of the Magnesum Brmngnate solution. SPR is formed by the stimulation of a surface plasmon dipole, which is created by a combination of electromagnetic waves and oscillations in the free electron density on the metallic surface and in the membrane of the insulating medium. Ephemeral waves are incident light waves that can go to the location where a medium and a metal meet when light travels from a regular fiber to an NCF. The amount of total internal reflection determines how light diffuses. When light enters objects linked to a waveguide, it exists as an ephemeral wave that is partially transmitted. An ephemeral wave that will be impacted by the analysis travels through the metallic sheet under resonance circumstances. the surface plasma wave (SPW) stimulated by the metal's interaction with the cladding , or its wave vector. Part of the incoming light energy is rapidly absorbed when the phase-matching requirement is met because the electromagnetic fields of the evanescent wave and SPW are closely connected. As a result, the intensity of light that is reflected lessens, and the transmission spectrum experiences a sizable loss dip. Resonance wavelength is the correct term for the wavelength of the dip. Because SPW can only propagate near metal films, the resonance wavelength is extremely responsive to RI adjustments of the external analyte being monitored. As a result, when the RI of an analyte varies, the phase matching conditions also change, which causes the location of the resonance wavelength to vary. This is how Figure (3) is meant scientifically.

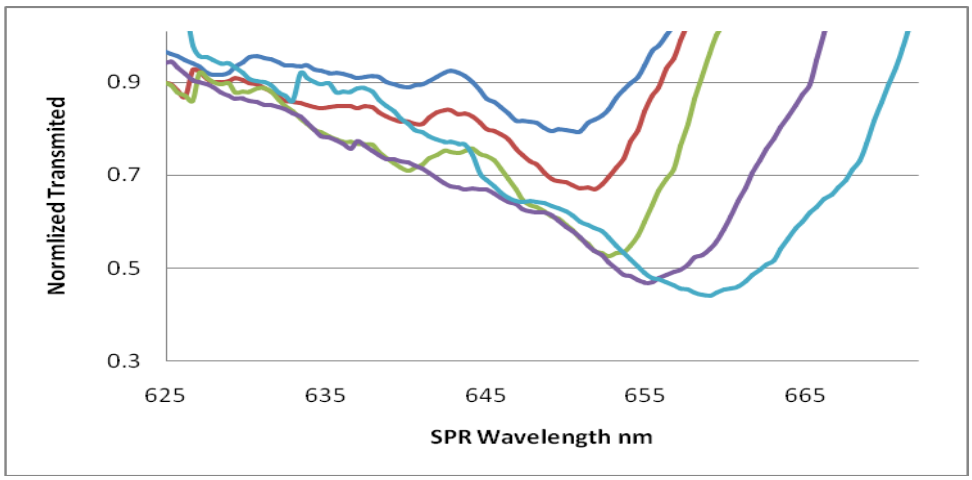

Figure (3) Resonant spectrum of the fiber/Au thin film SPR sensor using magnesium nitrate solution as analyte.

Figure 4 shows the linear fitting relationship between the analyte's refractive index and resonance wavelength when the sensor is using Magnesium Barmngnat solution as the analyte. The sensitivity of the fiber/Au film SPR sensor is 523 nm/RIU.

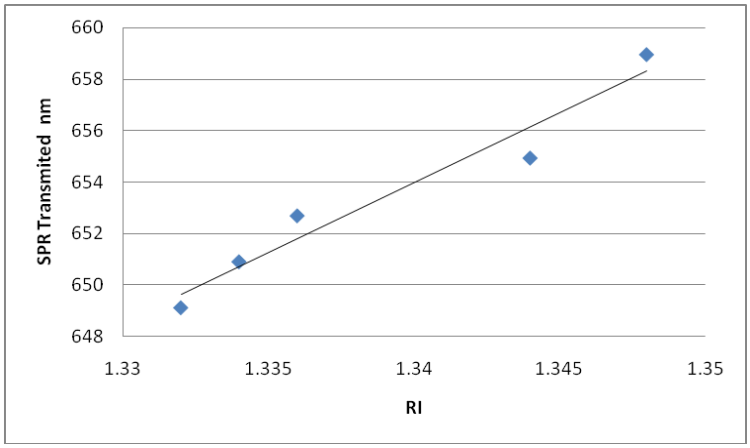

Figure (4) sensitivity fitting curve.

Figure (5) illustrates the intensity spectra of the laser beam transmitted from the coreless sensor coated with Au nanoparticle layer over the GO layer, where the intensity decreases with increasing concentration of the solution and evidence of RI (1.33 - 1.355).

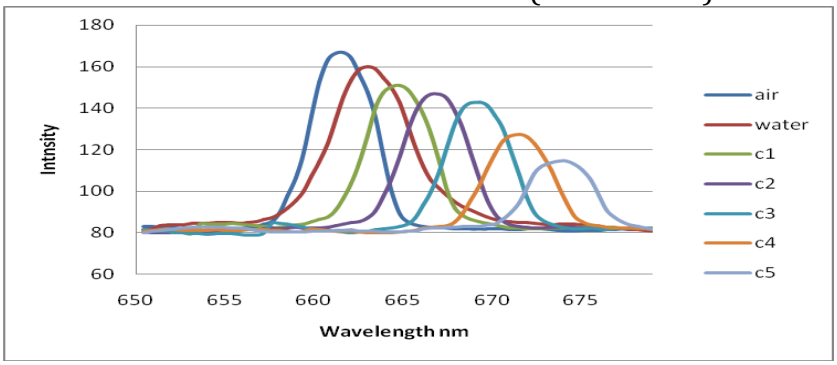

Figure (5) Transmission intensity of the Magnesium Barmngnat varies with wavelength when its refractive index is changed..

The resonant wavelength increases with increasing RI of the measuring medium. It moves into the red part of the spectrum, and the peak-to-trough distance steadily gets less. The SPR bottom

wavelength shift is examined to determine the sensor's refractive index when the medium to be measured's refractive index changes.

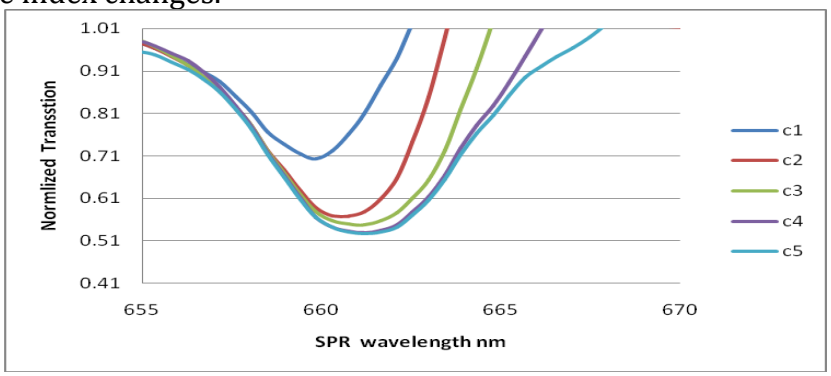

Figure (6) demonstrates how the transmission spectrum normalization and the resonance wavelength are related.

Figure (6) shows how the sensor's resonant wavelength shift changes when the liquid analyte's RI increases in the range (1.33–1.355).

The RI sensitivity curve of 1.33-1.355 is obtained, from the relationship between the change RI against the λ_{res} , maximum fiber sensitivity of the corresponding model enables from the graph of Figure (7) to 950 nm/RIU.

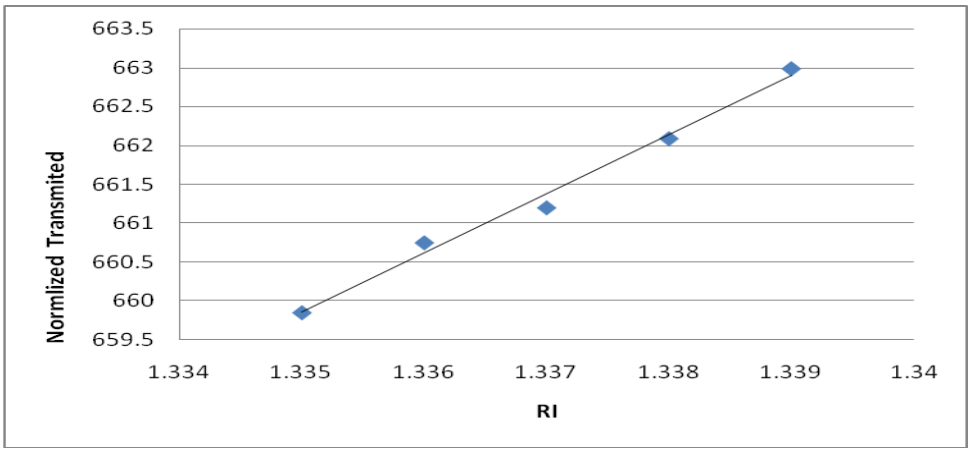

Figure (7) the sensitivity curve of Barmngnat solution .

Conclusion

An NCF-based SNCS sensor coated with a 20-nm-thick gold layer was suggested in this paper. The fundamentals of self-image sensing and multi-mode interferometry were investigated, and the operation of SNCS sensors with various refractive indices was explained. On the basis of NCF, the SNCS sensor was created. The gold-coated SM NC SM average sensor sensitivity is 523 nm/RIU, or 1.33 to 1.355. By measuring the response of a magnesium Barmanganat solution at 950 nm/RIU, the sensitivity of the GO-coated sensor was dramatically increased , It surpasses the structure of the conventional SNS by an order of magnitude. To create and enhance the detection of a Bermanganate sensor has a very low threshold concentration, the study initially concentrated on a sensor that is GO-sensitive as a foundation and an a test-driven approach. Controlling pollutants can help prevent environmental pollution.

Reference

1. 1-Wang, X.-D.; Wolfbeis, O.S. Fiber-optic chemical sensors and biosensors (2008-2012). Anal. Chem. 2013, 85, 487–508.
2. Xu, Y.; Lu, P.; Chen, L.; Bao, X. Recent developments in micro-structured fiber optic sensors. Fibers 2017, 5, 3.
3. Monzón-Hernández, D.; Villatoro, J.; Luna-Moreno, D. Miniature optical fiber refractometer using cladded multimode tapered fiber tips. Sens. Actuators B Chem. 2005, 110, 36–40.
4. Nath, P.; Singh, H.K.; Datta, P.; Sarma, K.C. All-fiber optic sensor for measurement of liquid refractive index. Sens. Actuators A Phys. 2008, 148, 16–18
5. 5-Wang, P.; Semenova, Y.; Wu, Q.; Farrell, G.; Ti, Y.; Zheng, J. Macrobending single-mode fiber-based refractometer. Appl. Opt. 2009, 48, 6044–6049.
6. 6-Zhang, X.; Peng, W. Bent-fiber intermodal interference based dual-channel fiber optic refractometer. Opt. Express 2015, 23, 7602–7610.
7. 7- Han, M.; Guo, F.; Lu, Y. Optical fiber refractometer based on cladding-mode Bragg grating. Opt. Lett. 2010, 35, 399–401
8. 8-Tien, C.-L.; Lin, H.-Y.; Su, S.-H. High sensitivity refractive index sensor by D-shaped fibers and titanium dioxide nanofilm. Adv. Cond. Matter Phys. 2018, 2018, 2303740.
9. 9- Minkovich, V.P.; Villatoro, J.; Monzón-Hernández, D.; Calixto, S.; Sotsky, A.B.; Sotskaya, L.I. Holey fiber tapers with resonance transmission for high-resolution refractive index sensing. Opt. Express 2005, 13, 7609–7614.
10. 10-Iga, M.; Seki, A.; Kubota, Y.; Watanabe, K. Acidity measurements based on a hetero-core structured fiber optic sensor. Sens. Actuators B Chem. 2003, 96, 234–238.
11. 11-Bao, Y.; Huang, Y.; Hoehler, M.S.; Chen, G. Review of fiber optic sensors for structural fire engineering. Sensors 2019, 19, 877.
12. Liang, L.; Ren, G.; Yin, B.; Peng, W.; Liang, X.; Jian, S. Refractive index and temperature sensor based on fiber ring laser with STCS fiber structure. IEEE Photonics Technol. Lett. 2014, 26, 2201–2204.
13. Yin, B.; Wu, S.; Wang, M.; Liu, W.; Li, H.; Wu, B.; Wang, Q. High-sensitivity refractive index and temperature sensor based on cascaded dual-wavelength fiber laser and SNHNS interferometer. Opt. Express 2019, 27, 252–264.
14. 14-Cao, S.; Shao, Y.; Wang, Y.; Wu, T.; Zhang, L.; Huang, Y.; Zhang, F.; Liao, C.; He, J.; Wang, Y. Highly sensitive surface plasmon resonance biosensor based on a low-index polymer optical fiber. *Opt. Express* **2018**, *26*, 3988–3994.
15. 15- Liu, Y.; Qu, S. Optical fiber Fabry-Perot interferometer cavity fabricated by femtosecond laser-induced water breakdown for refractive index sensing. *Appl. Opt.* **2014**, *53*, 469–474.
16. J. G. Aguilar-Soto, J. E. Antonio-Lopez, J. J. Sanchez-Mondragon, and D. A. May-Arrioja, "Fiber optic temperature sensor based on multimode interference effects," J. Phys. 274, 012011 (2011).
17. Q. Wang, G. Farrell, and W. Yan, "Investigation on singlemode-multimode-singlemode fiber structure," J. Lightwave Technol. 26, 512–519 (2008).
18. W. S. Mohammed, P.W. E. Smith, and X. Gu, "Wavelength tunable fiber lens based on multimode interference," J. Lightwave Technol. 22, 469–477 (2004).